ELSEVIER

Tectonic control for evaporite formation in the Eastern Betics (Tortonian; Spain)

Wout Krijgsman [a,*], Marianne E. Leewis [a], Miguel Garcés [b], Tanja J. Kouwenhoven [c], Klaudia F. Kuiper [a,d], Francesco J. Sierro [e]

[a] *Paleomagnetic laboratory "Fort Hoofddijk", Budapestlaan 17, 3584 CD Utrecht, The Netherlands*
[b] *Group of Geodynamics and Basin Analysis, University of Barcelona, Campus de Pedralbes, 08028 Barcelona, Spain*
[c] *Department of Geology, Utrecht University, Budapestlaan 4, 3584 CD Utrecht, The Netherlands*
[d] *Department of Isotope Geology, VU Amsterdam, De Boelelaan 1085, 1081HV Amsterdam, The Netherlands*
[e] *Department of Geology, University of Salamanca, 37008 Salamanca, Spain*

Abstract

Tectonic uplift and sea level lowering are two proposed mechanisms to explain the development of thresholds in front of the widespread evaporite basins of the circum-Mediterrranean region during the Miocene. Here we apply a multi-disciplinary approach to the continuously marine sequences of the Murcia–Cartagena basin to investigate which mechanism is responsible for the Tortonian evaporites of the Eastern Betics. First we develop a high-resolution chronology for the Venta de la Virgen section by integration of biostratigraphic, magnetostratigraphic and isotopic dating results. Next we construct palaeobathymetry and geohistory curves for this section and the Abad composite of the Sorbas basin. We show that the apparent differential vertical motions between the two sections cannot be explained by sea-level change but only by local tectonics. The Murcia–Cartagena basin shows significant tectonic uplift during the late Tortonian and early Messinian, while the neighboring Fortuna basin was rapidly subsiding. We conclude that tectonic activity on the Alhama de Murcia Fault was responsible for the emergence of a threshold that finally led to evaporite formation in the Fortuna basin.
© 2006 Elsevier B.V. All rights reserved.

Keywords: Stratigraphy; Tectonics; Evaporites; Miocene; Mediterranean

1. Introduction

The Miocene palaeogeographic evolution of the circum-Mediterranean region has frequently resulted in favourable conditions for evaporite formation in many different basins, as exemplified by the Middle to Late Miocene salt deposits of the Red Sea basin (Evans, 1988; Rouchy et al., 1995), the Middle Miocene (Badenian) evaporites of the Parathethys (Babel, 1999; Peryt et al., 2004); the late Tortonian gypsum units of the Eastern Betics (Montenat, 1973; Krijgsman et al., 2000) and the famous evaporites (halite, potash, gypsum) of the Messinian Salinity Crisis (MSC) of the Mediterranean (Ryan and Hsü, 1973; Hsü et al., 1973). Most of these evaporites formed in transitional marine-continental environments during a phase of basin restriction. The water circulation at depth became limited, so that the inflow of marine waters from adjacent seas or oceans could not be compensated by the outflow of dense and

---

saline waters. The salinity of the water in the basin would then increase, which ultimately resulted in the formation of evaporites.

In all cases, some kind of sill or threshold in front of the basin is needed for such a drastic phase of basin restriction to evolve. There are generally two hypotheses that explain the emergence of these thresholds: tectonic uplift and/or sea level lowering. These two mechanisms are usually very difficult to separate in the evaporite basin itself, since the hypersaline conditions during deposition hamper accurate interpretation of palaeoclimate and palaeoenvironment. In the Mediterranean, many studies argued for sea level lowering as a cause for the Messinian Salinity Crisis (e.g. (Kastens, 1992; Clauzon et al., 1996). Data from the Atlantic basin, however, clearly showed that glacio-eustatic changes were not responsible for the onset of the Messinian evaporites (Hodell et al., 2001; Krijgsman et al., 2004). At present, a dominantly tectonic control is favoured for the isolation of the Mediterranean Sea from the open ocean (e.g. (Weijermars, 1988; Duggen et al., 2003), probably in concert with a superimposed effect of the ~400 kyr eccentricity cycle (Krijgsman et al., 1999).

In this paper, we will focus on the mechanisms that caused the restrictive phase in basin evolution leading to the evaporites associated with the so-called "Tortonian Salinity Crisis" of the Eastern Betics (Krijgsman et al., 2000). Key questions are whether or not sea-level fluctuations were of great importance or what type of tectonic mechanism was responsible. For this purpose, we have examined the continuously marine Miocene sedimentary sequences of the Murcia–Cartagena Basin, which are located outside (southeast) of the evaporite-bearing Fortuna Basin. We selected the Venta de la Virgen section for an integrated stratigraphic study, because this section is the only continuous deep-marine sedimentary sequence in SE Spain that straddles the late Tortonian and early Messinian time interval. In addition, we have constructed detailed palaeobathymetric curves for both the Venta de la Virgen section and the well-dated Abad composite of the Sorbas basin (Sierro et al., 2001). Consequently, we could quantify in which sense sea-level change or tectonic uplift is a controlling factor on basin restriction. Our interpretations will provide a better and more substantiated explanation for the cause of evaporite formation in the Eastern Betics and its underlying mechanism.

2. Geological background

The Miocene sedimentary basins of SE Spain are part of a series of Neogene–Quaternary intramontane and foreland basins located in the Betic Cordillera. This mountainous range was formed during Alpine orogenesis in response to the closure of the Tethys. The Betic orogen can be subdivided into Internal Zones, External Zones, the Campo de Gibraltar Complex and the Neogene–Quaternary basins (Fig. 1). The External Zones, or South-Iberian Palaeomargin, are composed of two main palaeogeographic domains: Prebetic to the north and Subbetic to the south. The Internal Zones, or Alborán Microplate (Andrieux et al., 1971), are formed from bottom to top of three tectonically superimposed complexes: the Nevado-Filábride, the Alpujárride and the Maláguide. The Neogene basins formed in the Internal and External zones during the Early and Middle Miocene, under an overall NNW–SSE compressional regime related to Africa–Europe plate convergence and the collision of the Alboran Microplate against the South-Iberian Palaeomargin. Synorogenic (Early–Middle Miocene) and/or postorogenic (Late Miocene–Quaternary) sediments are unconformably overlying the folded and faulted substratum. The basins became progressively individualized in the emerging mountain chain and were bounded by many existing faults that thus preshaped the basins. Only in the late Miocene, vertical movements became of sufficient importance to define the present-day basin configuration (López-Garrido et al., 1998; Montenat et al., 1990a; Sanz de Galdeano and Vera, 1992).

In these Neogene–Quaternary basins, much research has been directed to the Late Miocene deposits because they could provide valuable clues and answers concerning the causes and consequences of the Messinian Salinity Crisis (e.g. (Martín and Braga, 1994; Rosell et al., 1998; Rouchy and Saint Martin, 1992; Fortuin and Krijgsman, 2003). In addition, the largely regressive sedimentary sequences of the Lorca and Fortuna basins (Fig. 1) were shown to contain evaporites that were substantially older than their MSC equivalents (Playà, 1998; Playà et al., 2000). Until recently, these evaporites were still considered to be of Messinian age (Müller and Hsü, 1987; Rouchy et al., 1998; Dinarés-Turell et al., 1999), but integrated magnetostratigraphic, biostratigraphic (fossil mammals and foraminifera) and cyclostratigraphic studies showed that the onset evaporite formation in the Lorca and Fortuna basins is dated at 7.80 ± 0.05 Ma, i.e. during the late Tortonian (Krijgsman et al., 2000). This age is in good agreement with a recently obtained $^{40}Ar/^{39}Ar$ age of 7.71 ± 0.11 Ma on the volcanic rocks that are intercalated just above the evaporites in the sedimentary sequence of the Fortuna basin (Kuiper et al., in press). The so-called "Tortonian Salinity Crisis" of the Eastern
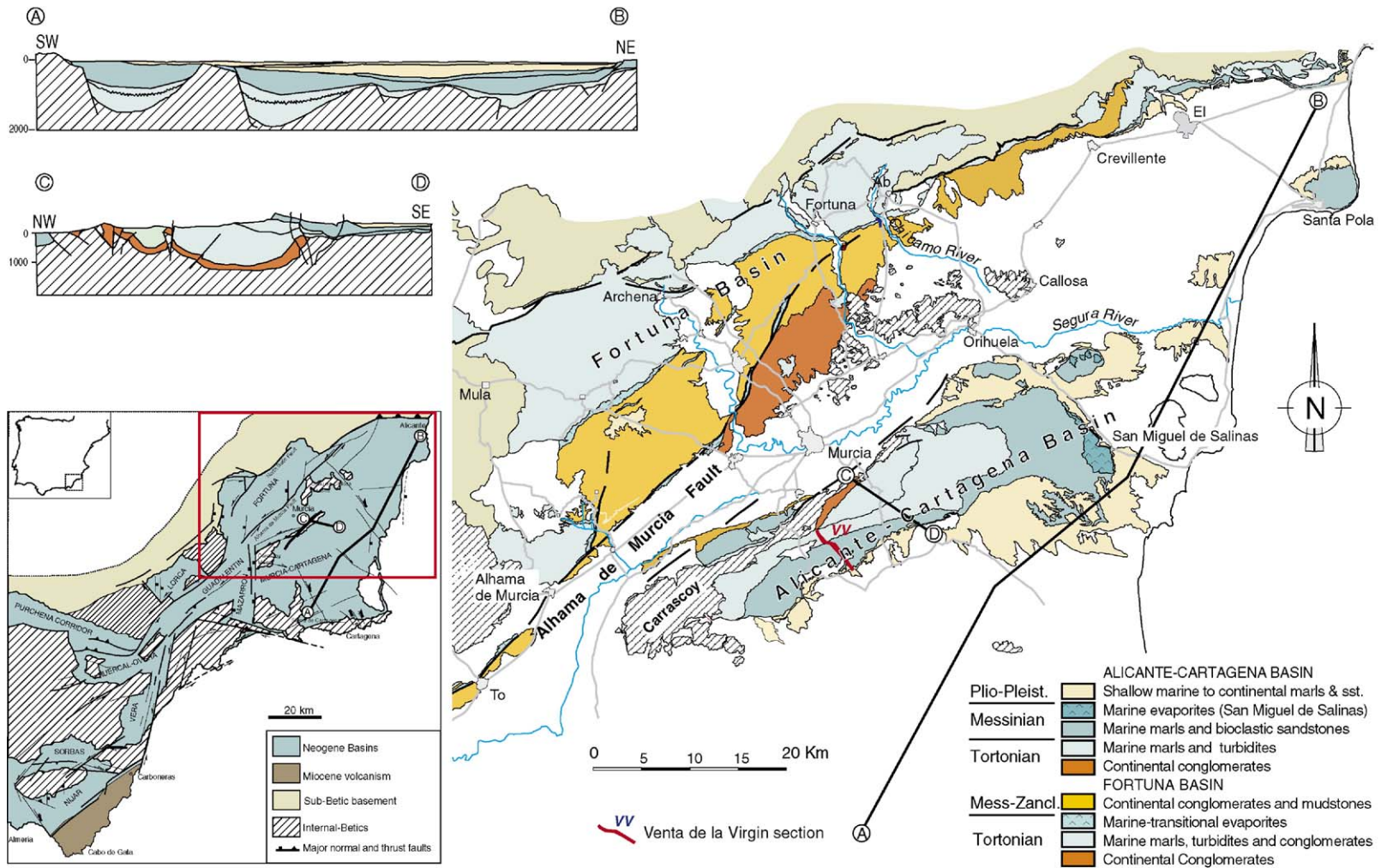
Fig. 1. Geological and structural setting of the Murcia–Cartagena basin in the eastern Betic Cordillera and simplified cross-sections AB and CD through the basin (after Montenat et al., 1990a,b and Garcés et al., 2001).

Betics has lasted for approximately 200 kyr, until an age of 7.6 Ma (Krijgsman et al., 2000), and the entire Messinian interval in the Fortuna basin is represented by continental facies (Garcés et al., 2001). The initiation of hypersaline conditions was suggested to be related to the emergence of a south-eastern ridge, which might have been linked to tectonic deformation along the SW–NE striking Alhama de Murcia fault system (Garcés et al., 2001). Another possibility is that a significant sea level lowering may have created a submarine barrier that was shallow enough to produce evaporitic conditions in the marginal Fortuna basin.

3. The Venta de la Virgen section

The Murcia–Cartagena basin is located southeast of the Fortuna basin and the Alhama de Murcia fault system on the western margin of the Mediterranean, north of the Alboran Sea (Fig. 1). This fault system belongs to the Betic segment of the lithospheric Trans-Alborán shear zone (De Larouzière et al., 1988). The Murcia–Cartagena basin is at present a large plain, bordered to the north by the Alicante and Crevillente Ranges (External Zones) and to the south by the Cartagena/Mazarron Mountains (Internal Zones). The basement in the Venta de la Virgen region belongs to the Internal Zones and is made up of schists, marbles and ophites. On top of this basement lies a sedimentary sequence, starting with a series of marine turbidites, breccias and marls, attributed to the early Tortonian (Tortonian I of Montenat et al., 1990a). They are separated by an angular unconformity from marine marls (and turbidites) of the late Tortonian (Tortonian II) to Messinian (Fig. 1). The Pliocene consists of continental deposits, which are in turn capped by Plio–Pleistocene conglomerates. In the vast structural anticline of the Triassic Carrascoy Massif only the Tortonian–Messinian marine series is present (Fig. 1); it is deposited here on top of continental breccias and red conglomerates (Montenat et al., 1990b).

The Venta de la Virgen section is situated along the southern flank of the Sierra de Carrascoy in the Murcia–Cartagena basin, SE of the city of Murcia (Fig. 1). It is located in a valley system between the Sierra de Los Villares (to the south) and the Umbría de los Sánchez (north of the Urbanización Mosa Trajectum). The section is named after the old village of Venta de la Virgen and is located east of highway N301 between Murcia and Cartagena, to the north of road C3319 toward San Javier, located on the Mediterranean coast.

The Venta de la Virgen section is primarily composed of a thick marine marl sequence, intercalated with banded sandstone deposits of Tortonian to Messinian age (Torremendo Formation of Montenat et al., 1990b). We have constructed a composite of 4 subsections (VV1 to VV4). The subsections were correlated to each other by laterally tracing of marker beds. The VV1 section starts with reddish clays overlying the basal conglomerates of the basin (Fig. 2). It gradually changes into a marine marl sequence with some sand layers and two intercalations of volcanic levels (VV2). The middle part (VV3) of the section shows a cyclic alternation of blue and yellowish marls with some fine-grained sandy intercalations. The upper part (VV4) is entirely made up of grey and white marls and displays evidence of major slumping towards the top. The marl sequences are capped by a well-stratified sandstone unit (La Virgen Formation of Montenat, 1990).

4. Integrated stratigraphic results

4.1. Biostratigraphy

A series of foraminiferal bioevents was identified in the Venta de la Virgen section based on the distribution of Globorataliids and Neogloboquadrinids. These events were useful to correlate this section with other classical Mediterranean sections such as the Abad composite of the Sorbas basin (Sierro et al., 2001).

Foraminiferal preservation was not good in the lowermost part of the Venta de la Virgen section, but we were able to identify *Globoratalia menardii* form 4 (sinistral), which was continuously present and relatively abundant in the lower part of VV1 (15–85 m). Upwards in the stratigraphy, this species is absent or scarce with the exception of three brief influxes that have been identified at around 115 m in VV1, at 32 m and 100 m in VV2 where this species is abundant again. The intermittent distribution of this species in the upper part of section VV1 and lower part of section VV2 makes it more difficult to use it as a reliable biostratigraphic marker, but we have tentatively correlated the brief reoccurrence of the species at the 32 m level in section VV2 with the last common occurrence (LCO) of *G. menardii* form 4 (M4 in Fig. 2), using the same criteria as in the central and east Mediterranean sections (Krijgsman et al., 1995). The top of the interval where this species regularly occurs is located at around meter 85 (M4a in Fig. 2).

In section VV2, we identified the First Common Occurrence (FCO) of *G. menardii* form 5 (dextral) (M5 in Fig. 2) that occurs at 103 m. This species is relatively common up to circa 125 m where the group of *Globorotalia miotumida* becomes abundant (GM in Fig. 2).
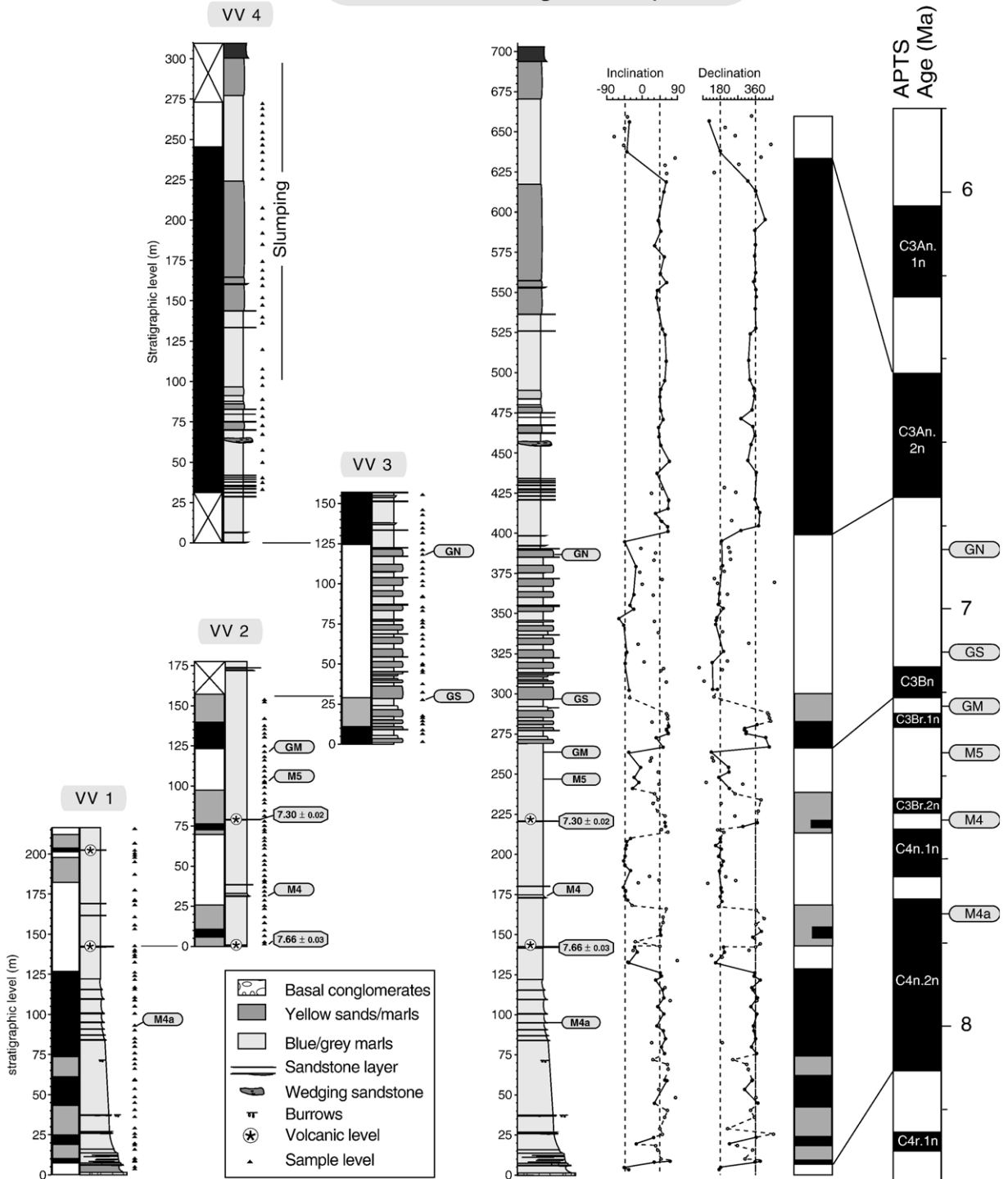
Fig. 2. Magnetic polarity, lithology, biostratigraphic events, declination/inclination results and correlation to the APTS of the Venta de la Virgen composite, which is composed of four subsections (VV1–VV4). In the polarity column black (white) denotes normal (reversed) polarity. The bioevents correspond to M4a = top of *G. menardii* 4 interval, M4 = *G. menardii* 4 LCO, M5 = *G. menardii* 5 FO, GM = *G. miotumida* group FRO, GS = sinistral *G. scitula* LCO, GN = *G. nicolae* FO.

The First Regular Occurrence (FRO) of this species closely corresponds to the Tortonian–Messinian boundary (Hilgen et al., 2000). Specimens of the *G. miotumida* group are abundant to the top of the VV2 section and become intermittent from 115 to 130 m in section VV3.

The group of *Globorotalia scitula* is constantly present in VV1 and VV2. The Last Common Occurrence of *G. scitula* (sinistral) has been located in the lower part of section VV3 at 27 m (GS in Fig. 2). This bioevent was also identified in the Sorbas basin (Sierro et al., 2001). Specimens of *G. scitula* (dextral), although scarcer than the sinistral forms, are present in the lower part of VV3 up to 50 m, where the last common occurrence of the species was located.

The interval above 50 m in VV3 is devoid of unkeeled Globorotaliids, which reappear again at 120 m where the First Occurrence of *Globorotalia nicolae* was identified (GN in Fig. 2). This species is relatively common although intermittent from 120 to 140 m.

A significant change in benthic foraminiferal assemblages was identified in the uppermost part of section VV3 above meter 145. Uvigerinids start to be very abundant along with shallow-water benthic foraminifera. *Uvigerina cylindrica*, which appears in Sorbas near the boundary between the "Lower Abad" and "Upper Abad" was identified here in this uppermost part of VV3.

With a few exceptions, planktonic foraminifera were scarce in most samples of VV4. The residues were very small and benthic foraminifera were the dominant fraction. This dominance of benthonic specimens in the foraminiferal assemblage is already evident in the uppermost part of VV3. Because we found no specimens of *G. nicolae* in VV4, nor in the topmost samples of VV3, we assume that VV4 was deposited above the top of the *G. nicolae* zone which defines in Sorbas the limit between the "Lower Abad" and "Upper Abad" (Sierro et al., 2001).

Although sinistral and dextral specimens of *Neogloboquadrina acostaensis* coexist in VV4, we assume that the change in coiling from sinistral to dextral in *N. acostaensis* is not reached and that the presence of dextral *N. acostaensis* is probably due to reworking of old Lower or Middle Tortonian Neogloboquadrinids into the Messinian. Reworking or slumping might also explain the abundant occurrence of *G. miotumida* in short intervals around 50 and 150–160 m in VV4, although some of these levels may be related with the brief influxes of this species observed in the Sorbas basin in the lower part of the "Upper Abad" (Sierro et al., 2001).

4.2. Magnetostratigraphy

The natural remanent magnetization (NRM) of the samples was measured on a 2G Enterprise DC SQUID cryogenic magnetometer. The specimens were thermally
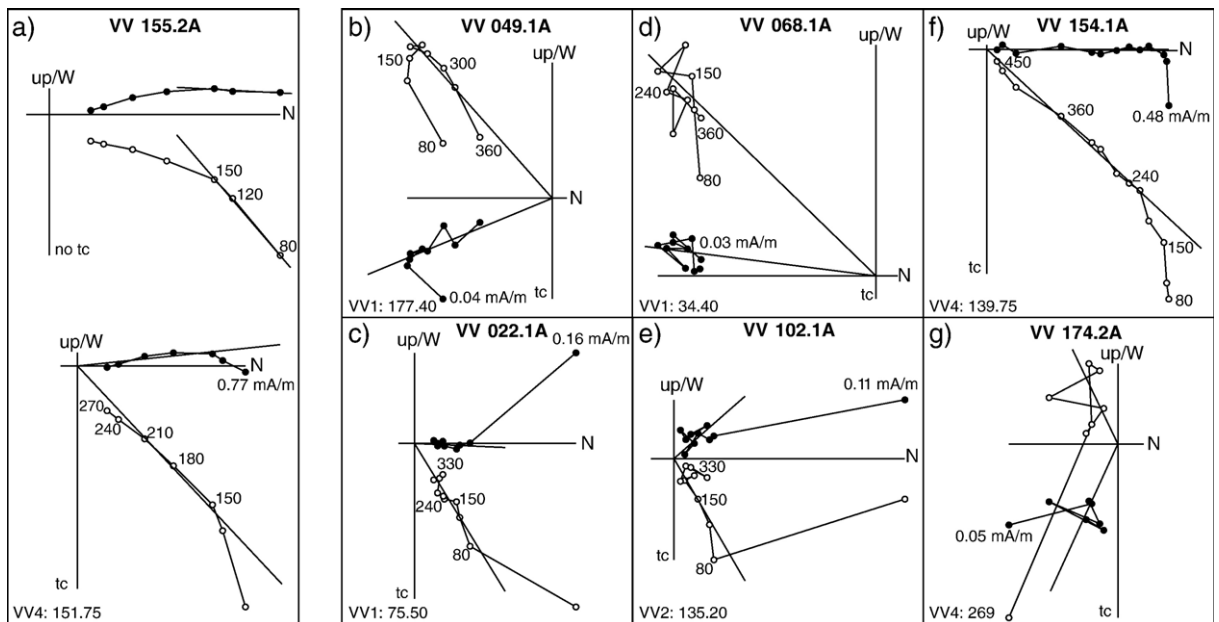

Fig. 3. Zijderveld diagrams of thermal demagnetisation. Closed (open) symbols represent the projection of the vector end-points on the horizontal (vertical) plane; values represent temperature in °C and NRM intensity (mA/m); stratigraphic levels are in the lower left-hand corner. The diagrams are represented without (no tc) or with tectonic correction (tc).
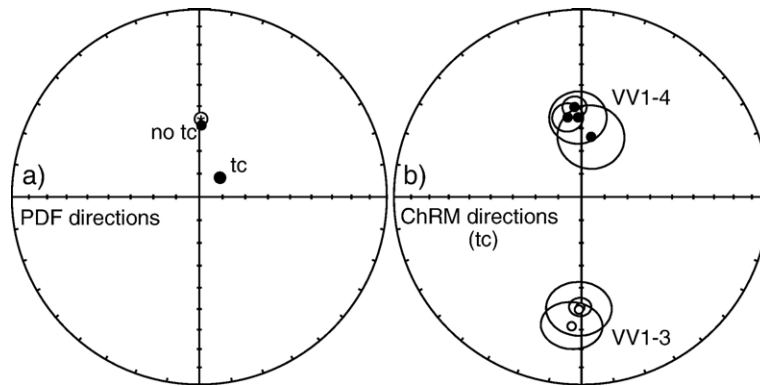
Fig. 4. Equal area projections of the section mean directions. a) Low temperature present-day field overprint component (VV4) before (no tc) and after (tc) bedding tilt correction. Star denotes the present-day direction ($I=57°$) for the Venta de la Virgen section (latitude of 38 °N). b) High-temperature ChRM component (VV1–VV4) after bedding tilt correction. Ellipses denote the 95% confidence regions around the mean directions. Statistical results are given in Table 1.

demagnetised using 20–50 °C steps. NRM directions were determined using principal component analysis (Kirschvink, 1980) and the results were plotted in orthogonal demagnetisation plots (Zijderveld, 1967). Declination and inclination were calculated for each characteristic component stable endpoint direction after correction for bedding tilt. Mean directions were determined for all subsections using standard Fisher statistics.

The intensities of many samples were very low (0.01–0.5 mA/m with only few samples having higher intensities) and it was therefore not always easy to reliably determine the characteristic components. Apart from a randomly oriented laboratory-induced component removed between 80 and 120 °C we could discern a normal polarity component, which was removed below 210 °C and has a present-day field orientation in geographical coordinates (Fig. 3a). We interpreted this component as a (sub)recent present-day field (pdf) overprint. Mean directions of this pdf-component calculated without tilt correction are well clustered with average inclination in close agreement with the present-day latitudinal position of the Murcia–Cartagena basin (Fig. 4a; Table 1). The remainder of the magnetic signal appeared to be of dual polarity and was generally removed between temperatures of 300 and 360 °C in sections VV1 to VV3, but at slightly higher temperatures (up to 450 °C) in section VV4 (Fig. 3g). We have interpreted this component as the characteristic remanent magnetization (ChRM) component.

Despite low intensities, a significant part of the samples show relatively good results (Fig. 3b,c,d,f), with the demagnetisation components revealing a (more or less) linear decay towards the origin. Other demagnetisation diagrams do not show such a clear

linear decay, but are still good enough to determine the primary polarity (Fig. 3e,g). Samples were considered uninterpretable when demagnetisation curves show too much scatter in different directions. Declinations and inclinations were calculated for each characteristic component stable endpoint direction. The ChRM directions and polarity zones of the Venta de la Virgen composite show that at least six polarity reversals have been recorded: three normal polarity zones and four reversed polarity zones (Fig. 2). Mean directions for the ChRM component were calculated for all four subsections, which appear to be in good agreement (Fig. 4b, Table 1). The overall mean direction is: Decl. = 358°, Incl. = 48°, indicating that no significant vertical axis rotation has taken place since the late Tortonian, similar to the other Miocene basins of southern Spain

Table 1
Results from paleomagnetic analysis of the different subsections of Venta de la Virgen

Section	Pol.	N	Decl.	Incl.	k	a95
VV-III+IV	pdf	45	1.6	58.6	86.7	2.3
	pdf (tc)	45	47.7	78.0	86.6	2.3
VV-I	N	24	350.2	54.5	22.2	6.4
	R	10	184.4	−31.5	18.2	11.7
VV-II	N	10	357.5	54.9	17.5	11.9
	R	13	180.7	−40.9	90.7	4.4
VV-III	N	6	9.0	63.4	23.4	14.2
	R	9	181.3	−39.8	17.0	12.9
VV-IV	N	24	355.6	50.2	37.0	4.9
VV-all	N	64	354.8	53.9	24.3	3.7
	R	33	182.0	−37.6	26.8	4.9
VV	N+R	97	357.8	48.4	20.4	3.3

Pol. = polarity (N = normal, R = reversed); N = number of specimens; Decl. = declination; Incl. = inclination; k = Fisher's precision parameter; α_{95} = 95% cone of confidence, pdf = present-day field component. The results are plotted in equal area projections in Fig. 4.

([Krijgsman and Garcés, 2004](#)). The inclinations are too shallow for the palaeogeographic latitude of the Murcia–Cartagena basin in the late Miocene, which suggests that the primary magnetic signal has been affected by sedimentary inclination errors.

4.3. Isotopic dating

Samples for ^{40}Ar/^{39}Ar dating were collected at two different volcanic levels in the VV2 section ([Fig. 2](#)). The bulk samples were washed and sieved, and the fractions of 400–500 μm were used for standard magnetic and heavy liquid separations for sanidine. Subsequently, the samples were handpicked, leached with a 1:5 HF solution and loaded in a 5 mm ID quartz vial together with Fish Canyon Tuff (FC-2) sanidine. The vial was irradiated in the Oregon State University TRIGA reactor in the cadmium shielded CLICIT facility for 7 h. The FC-2

standards and the Venta de la Virgen sanidine samples have been preheated using a defocused laser beam to remove undesirable atmospheric argon and were consequently analysed by total fusion with a Mass Analyzer Products LTD 215-50 noble gas mass spectrometer. The ^{40}Ar/^{39}Ar dating was performed according to standard laboratory procedures (for more details see [Kuiper et al., in press](#)) and all ^{40}Ar/^{39}Ar ages have been calculated using the decay constants of [Steiger and Jäger (1977)](#). The age for Fish Canyon Tuff sanidine used in age calculations is 28.02 Ma ([Renne et al., 1998](#)). Correction factors for neutron interference reactions are $2.64 \pm 0.017 \times 10^{-4}$ for $(^{36}Ar/^{37}Ar)_{Ca}$, $6.73 \pm 0.037 \times 10^{-4}$ for $(^{39}Ar/^{37}Ar)_{Ca}$, $1.211 \pm 0.003 \times 10^{-2}$ for $(^{38}Ar/^{39}Ar)_K$ and $8.6 \pm 0.7 \times 10^{-4}$ for $(^{40}Ar/^{39}Ar)_K$. Errors are quoted at the 1σ level and include the analytical error and the error in J.

The results of the ^{40}A/^{39}Ar total fusion experiments of the Venta de la Virgen samples 2000V1 and 2000V2
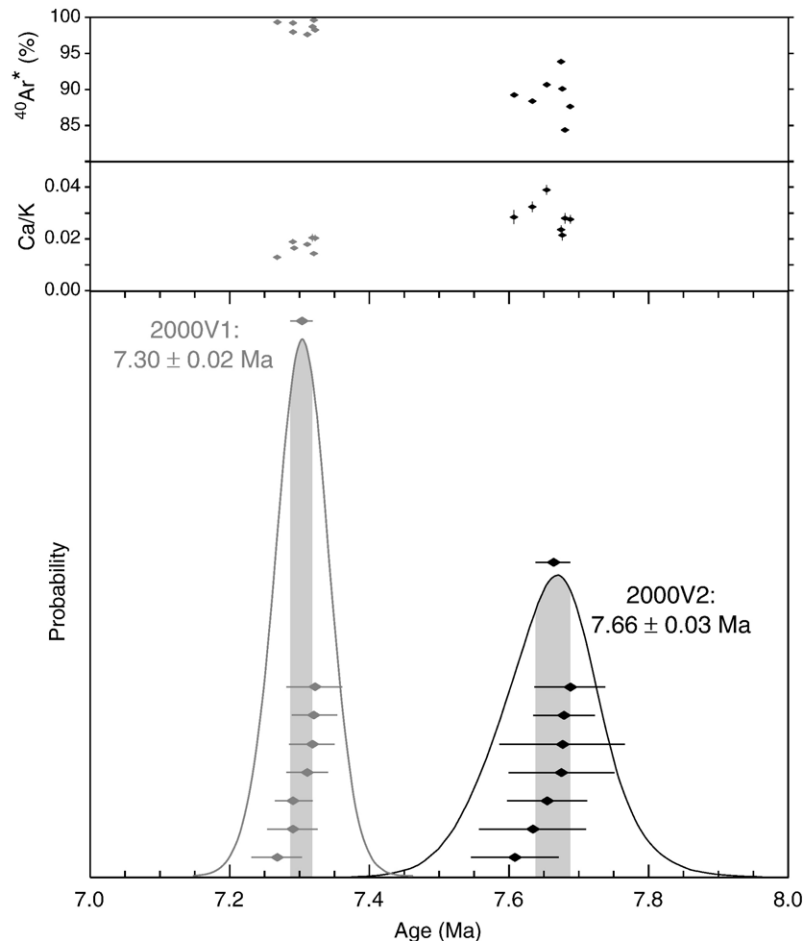

Fig. 5. Age distributions of ^{40}Ar/^{39}Ar data. All single fusion experiments are indicated as black and grey squares for respectively 2000V2 and 2000V1. The weighted mean ages are indicated at the top of the distribution curves. The shaded area represents the standard error. Sample 2000V2 shows a very slight tailing towards the younger end. Additionally, radiogenic ^{40}Ar yields and Ca/K ratios are shown.

Table 2
^{40}Ar/^{39}Ar data of total fusion experiments

VU-ID	^{36}Ar$_A$	^{37}Ar$_{Ca}$	^{38}Ar$_{Cl}$	^{39}Ar$_K$	^{40}Ar*	Age (Ma) ±1σ	^{40}Ar* (%)	Ca/K ± 1σ	^{40}Ar*/^{39}Ar$_K$ ± 1σ Sample	^{40}Ar*/^{39}Ar$_K$ ± 1σ Standard
	×10^{-15} mol									
2000V1										
01M0414A	0.00273	0.14860	0.00072	18.26083	38.81131	7.29±0.04	97.92	0.0189±0.0011	2.1254±0.0106	8.2184±0.0123
01M0414C	0.00061	0.07536	0.00100	13.57105	28.75525	7.27±0.04	99.34	0.0129±0.0011	2.1189±0.0106	8.2184±0.0123
01M0414D	0.00035	0.08626	0.00000	14.02815	29.94356	7.32±0.03	99.62	0.0143±0.0010	2.1345±0.0097	8.2184±0.0123
01M0414E	0.00253	0.11333	0.00000	14.70320	31.34138	7.31±0.03	97.63	0.0179±0.0009	2.1316±0.0088	8.2184±0.0123
01M0414F	0.00120	0.15274	0.00000	21.49398	45.69388	7.29±0.03	99.19	0.0165±0.0007	2.1259±0.0080	8.2184±0.0123
01M0414H	0.00138	0.12935	0.00121	14.70910	31.38398	7.32±0.03	98.68	0.0205±0.0015	2.1336±0.0096	8.2184±0.0123
01M0414I	0.00176	0.12056	0.00186	13.75671	29.36656	7.32±0.04	98.22	0.0204±0.0013	2.1347±0.0118	8.2184±0.0123
						Weighted mean: **7.30 ± 0.02**			Normal isochron intercept: 260±64	
						MSWD: 0.34			inverse isochron intercept: 336±76	
2000V2										
01M0418A	0.00813	0.17478	0.00000	10.44253	23.43114	7.69±0.05	90.67	0.0389±0.0018	2.2438±0.0148	8.2246±0.0123
01M0418B	0.01034	0.14456	0.00000	10.38961	23.28781	7.68±0.04	88.37	0.0324±0.0020	2.2415±0.0130	8.2246±0.0123
01M0418D	0.00897	0.09974	0.00000	10.78572	24.16315	7.67±0.08	90.09	0.0215±0.0022	2.2403±0.0221	8.2246±0.0123
01M0418E	0.00786	0.10536	0.00000	8.62316	19.32073	7.68±0.09	89.23	0.0284±0.0027	2.2406±0.0263	8.2246±0.0123
01M0418G	0.01328	0.11459	0.00000	9.54067	21.25772	7.63±0.08	84.39	0.0279±0.0021	2.2281±0.0226	8.2246±0.0123
01M0418H	0.01192	0.13329	0.00143	11.25105	24.98331	7.61±0.06	87.61	0.0276±0.0017	2.2205±0.0184	8.2246±0.0123
01M0418I	0.00632	0.13057	0.00000	12.88186	28.78108	7.65±0.06	93.87	0.0236±0.0017	2.2342±0.0168	8.2246±0.0123
						Weighted mean: **7.66 ± 0.03**			Normal isochron intercept: 290±27	
						MSWD: 0.22			inverse isochron intercept: 287±27	

Errors are 1 sigma analytical errors, and in bold weighted mean age and standard error are given.

are given in Fig. 5 and Table 2. In both cases 7 multiple (5–10)-grain fractions have been analysed. For sample 2000V2 the percentage radiogenic ^{40}Ar is on average 89.1%, which is relatively low for sanidine. The average radiogenic ^{40}Ar content for 2000V1 is 98.7%. The individual analyses are concordant at the 68% level and a weighted mean age and standard error are calculated as the crystallization ages. The isochron ages are concordant with the weighted mean age and the trapped ^{40}Ar/^{36}Ar component is atmospheric. This yields an age of 7.30±0.02 Ma for 2000V1 and 7.66±0.03 Ma for 2000V2 (Fig. 5; Table 2). Errors increase to respectively ±0.08 Ma and ±0.08 Ma when uncertainties in the age of the primary standard and decay constants are included (Renne et al., 1998).

5. Chronology for the Venta de la Virgen section

High-resolution biostratigraphic records from astronomically dated Late Miocene sections have earlier demonstrated that numerous planktonic events are synchronous all over the Mediterranean basin (Hilgen et al., 1995; Hilgen and Krijgsman, 1999; Sierro et al., 2001). Several of these events have been recognised in the Venta de la Virgen section and they may thus serve as excellent first-order chronologic calibration points. The astronom-

ical ages of these events comprise in stratigraphic order: 1) the (sinistral) *G. menardii 4* LCO at 7.512 Ma, 2) the (dextral) *G. menardii 5* FO at 7.355 Ma, 3) the *G. miotumida* group FRO at 7.240 Ma, 4) the sinistral *G. scitula* LCO at 7.095 Ma, and 5) the *G. nicolae* FO at 6.829 Ma (Fig. 2). In addition, the general presence of *G. menardii 4* in the lowermost (15–85 m) part of the section indicates that it is older than 7.726 Ma (Hilgen et al., 1995). At the transition from VV3 to VV4 there is a significant change in benthic assemblages, with Uvigerinids and shallow-water species starting to be abundant. The sudden appearance of *Uvigerina cyclindrica* occurs here as well, which may allow a direct correlation to the "Lower/Upper Abad" transition in the Sorbas basin (∼6.8 Ma). The uppermost part of the section VV4 is less straightforward because foramifera are rare, sedimentary slumping is common and samples probably include reworking of older fauna. Nevertheless, the observed faunal assemblages suggest that VV4 is most likely related to the lowermost part of the "Upper Abad", below the sinistral/dextral coiling change of *N. acostaensis* at 6.337 Ma (Hilgen et al., 1995). Consequently, our biostratigraphic data suggest that the entire sequence was deposited between at least ∼7.8 and ∼6.4 Ma.

The magnetostratigraphic polarity pattern of the Venta de la Virgen section is not very well established

and a straightforward correlation to the GPTS cannot be made without additional age constraints. Our biochronological data indeed suggest that several reversals and short polarity subchrons must have been missed. Nevertheless, some characteristics in the polarity pattern are very helpful to improve the chronology of the section. The lowermost part of the VV1 section clearly shows evidence for reversed polarities. Regarding the general presence of *G. menardii* 4 directly above this interval, it implies that the observed R–N reversal at the base of the sequence most likely corresponds to the base of chron C4n.2n at ∼8.1 Ma. In addition, the normal polarity interval between the *G. miotumida* FRO and the sinistral *G. scitula* LCO agrees very well with the position of the normal chron C3Bn in other Mediterranean sections (Hilgen et al., 1995). The R–N reversal at the top of VV3 slightly follows the *G. nicolae* FO, indicating that the normal polarity interval of VV4 corresponds to C3An.2n (Krijgsman et al., 1999; Sierro et al., 2001). The top of section VV4 reveals again evidence of reversed polarities, which indicates that the base of the reversed chron C3An.1r at 6.44 Ma is just reached. It cannot be completely excluded that these reversed polarities may correspond to chron C3r, but this option is not supported by our magnetostratigraphic and biostratigraphic data. The Venta de la Virgen magnetostratigraphy is thus especially helpful to provide better age constraints on the base and top of the section, allowing more accurate calculations of sediment accumulation rates (Fig. 6). It furthermore shows that the Venta de la Virgen section comprises a time interval of about 1.7 Myr. This suggests that our

average sample resolution was in the order of 10 kyr, which could be an explanation why several short (∼20 kyr) subchrons have been missed in the polarity pattern of Venta de la Virgen.

The isotopic dating results of the two volcanic levels in section VV2 provide extra age control on the sedimentary sequence and confirm the other age ascriptions for the Venta de la Virgen section. The ^{40}Ar/^{39}Ar age of 7.30±0.08 Ma for 2000V1 is in close agreement with its location in chron C3Br.2r (7.454–7.285 Ma) and its position near the *G. menardii* 5 FCO event at 7.355 Ma. The age of 7.66±0.08 Ma for 2000V2 concords with the dominantly normal polarities of C4n, and is considerably older than the *G. menardii* 4 LCO at 7.512 Ma which occurs at a higher stratigraphic level. In other Mediterranean sections, *G. menardii* 4 is commonly present until 7.726 Ma, but is absent in the interval 7.726–7.545. The top of the *G. menardii* 4 interval in VV1 (event M4a) could thus correlate to 7.726 Ma, which is in agreement with the palaeomagnetic and isotopic data. These correlations concur with the general picture of rather continuous sediment accumulation rates in the Neogene basins of the eastern Betics (Fig. 6).

6. Palaeobathymetric analyses

6.1. Method

We performed a palaeobathymetric analysis on the sedimentary sequences of both the Venta de la Virgen and the Abad composite of the Sorbas basin to
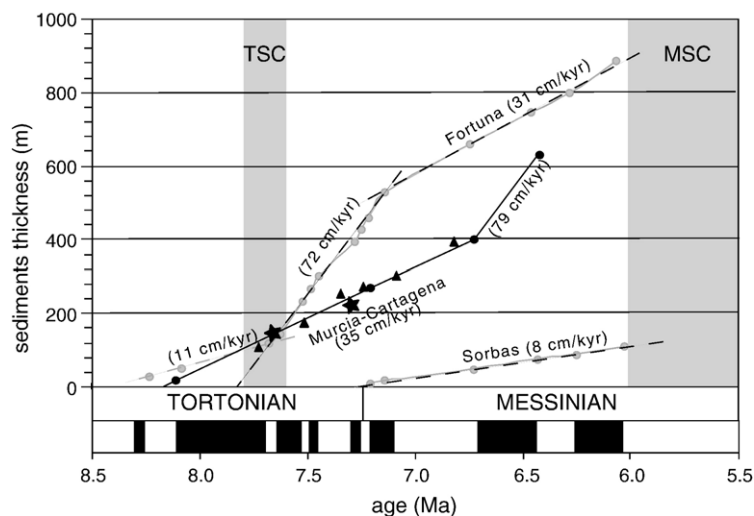

Fig. 6. Sedimentation rates of the Venta de la Virgen section in the Murcia–Cartagena basin, compared to the composite sedimentation curves of the Fortuna basin (after Garcés et al., 2001) and the Sorbas basin (after Sierro et al., 2001). TSC refers to the "Tortonian Salinity Crisis" interval in the eastern Betics according to Krijgsman et al. (2000) MSC refers to the Messinian Salinity Crisis of the Mediterranean.

reconstruct sea level fluctuations and vertical motions. The method used is described in detail by Van Hinsbergen et al. (2005) and is based on the variation of foraminiferal faunas with depth: the percentage of planktonic foraminifera with respect to the total population (both planktonic and benthic foraminifera) generally increases with increasing water depth, which is represented by the regressional relationship determined by Van der Zwaan et al. (1990):

$$\text{Depth (m)} = e^{3.58718 + (0.03534 \, {}^* \%P)}$$

where the plankton fraction $\%P = 100 {}^* P/(P+B-S)$, with P the amount of planktonic foraminifera, B the amount of benthic foraminifera and S the amount of environmental stress markers (Van Hinsbergen et al., 2005), being benthic foraminifera that tolerate low oxygen levels (like several *Bolivina*, *Bulimina* and *Uvigerina* species). Sapropelitic samples and samples where the number of stress markers is higher than 60% ($S > 60\%$) are discarded. Counting procedures were done following Van Hinsbergen et al. (2005) and an independent taxonomy check, identifying depth marker species, was carried out on selected samples.

To construct the actual vertical motions from the calculated estimated palaeobathymetry we first used a 5 pt moving average to filter out the extreme values, and then performed backstripping procedures as described in Steckler and Watts (1978) and Van Hinte (1978), using initial thickness values from Perrier and Quibler (1974) and accounting for sediment accumulation and sea-level changes. A local isostasy model under the assumption of no flexural lithospheric response was adopted.
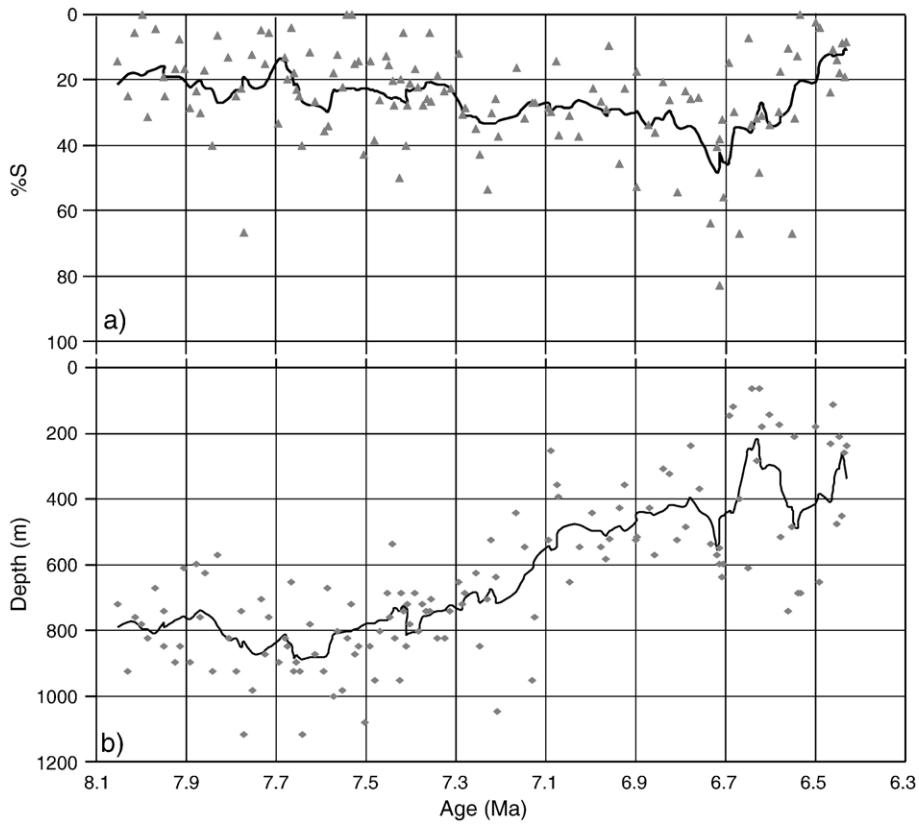
6.2. Results

The P/B ratios calculated for the Venta de la Virgen section show a significant decrease in palaeodepth through time. The independent taxonomy check also confirmed this trend, since the majority of the identified depth markers fall in the calculated range of the P/B ratio method (Fig. 7). This decrease in palaeodepth is coeval with an increase in the percentage of environmental stress markers (%S), suggesting that the basin environment became progressively restricted. A significant change with increasing %S occurs around 7.3 Ma ago, close to the Tortonian/Messinian boundary. From around 6.7 Ma ago the %S decreases again, although the decrease in palaeodepth continues (Fig. 7). From the vertical motions curve (Fig. 8) constructed from the palaeobathymetric data, it follows that the Venta de la Virgen area is subjected to a tectonic uplift with an

average uplift rate of 30 cm/kyr which started at ∼8 Ma ago and continued up to ∼6.6 Ma. At the start of the section an apparent initial subsidence can be seen, although this is probably a relic from the backstripping procedure. The youngest part of the section has also not been taken into account in the discussion as this corresponds with excessive slumping.

The Abad Composite of the Sorbas basin (Sierro et al., 2001) is divided into two units, the "Lower Abad" and the "Upper Abad". The samples of the "Lower Abad" section are of good quality, representing open marine conditions, and can be used for P/B ratio analysis. The samples of the "Upper Abad" are affected by large amplitude changes in the percentage planktonic foraminifera since no benthics exist in sapropels and no planktonic foraminifera in the middle of the homogeneous layers. The Upper Abad was thus discarded and not taken into account in the geohistory analysis of the Sorbas basin. Nevertheless, preliminary analysis, by trying to circumvent the foraminiferal assemblage problems, suggests that the "Upper Abad" marl series went through a shallowing phase and therefore an apparent uplift as the minor sediment load should not be able to suppress this uplift. The sedimentation rate (∼8 cm/kyr) continued to stay the same during the Lower and the Upper Abad series. The subsidence curve (Fig. 8) of the "Lower Abad" section shows that the Sorbas basin did not go through a significant uplift or subsidence between 7.2 and 6.7 Ma ago. The estimated palaeobathymetric depth of the Abad section based on the P/B method is quite deep (1000 m), in agreement with earlier results (Baggley, 2000). The benthic foraminiferal depth markers, however, provide depth estimates of only 400 ± 100 m. The latter value is in much better agreement with earlier palaeobathymetric estimates (e.g. 400 m (Dronkert, 1976); 200–300 m (Troelstra et al., 1980), 400–600 m (Poisson et al., 1999), max. 400 m (Vázquez et al., 1999).

7. Tectonic control for evaporite formation

Our palaeobathymetric results of the Venta de la Virgen section show a clear gradual decrease in palaeodepth through time (Fig. 7). If sea-level fluctuation had been responsible for this decrease it should also have affected the other basins in the Mediterranean. Our results from the Sorbas basin reveal no change at all, so we conclude that tectonism is a more likely explanation for the differential vertical motions between the two basins. The stress field in southeastern Spain changed during the late Tortonian, resulting in large-scale tectonic displacements along NE/SW trending

Fig. 7. a) Percentage of stress markers (%S) through time of the Venta de la Virgen section. Triangles represent actual calculated percentages per sample. The black line is constructed by using a 5-point moving average. b) Paleobathymetry curve (Depth) through time. Squares represent the estimated depth per sample by using the P/B ratio calculation. The black line is again constructed by using a 5-point moving average. c) The results of the independent taxonomy check on selected samples.

sinistral strike-slip faults (Stapel et al., 1996). The marine Sorbas and Nijar basins were formed resulting in the deposition of shallow marine calcarenites of the late Tortonian Azagador Member (Fortuin and Krijgsman, 2003). The Murcia–Cartagena basin has apparently experienced a gradual uplift between ∼8 and 6.7 Ma, which was primarily caused by local tectonics. This conclusion is also in agreement with the isotopic records of the Atlantic Ocean, which do not show any significant changes in $\delta^{18}O$ values during the late Tortonian (Hodell et al., 2001).

The palaeogeographic evolution of the Murcia–Cartagena basin shows several marked events, which now have been accurately dated. During Tortonian I, a relatively small basin was filled with breccias and red conglomerates (Fig. 1). This basin must have undergone a large subsidence in the early Tortonian as vast amounts of marine marls and turbidites were deposited on top of the basement or on the continental sediments. Our results from Venta de la Virgen show that the basin had an estimated palaeobathymetric depth of 800–1000 m at

the beginning of Tortonian II about ∼8 Ma ago (Figs. 7 and 8). During its gradual uplift in the late Tortonian, the Murcia–Cartagena basin remained in open contact with the Mediterranean until it became continental in the latest Messinian. Nevertheless, a marked event took place in the interval straddling the Tortonian/Messinian boundary at ∼7.3 Ma, where an increase in environmental stress markers (%S) reflects a change towards more restricted environments (Fig. 7). Another change in basin configuration took place around 6.7 Ma, with the initiation of slumping coinciding with a decrease in %S. Time-equivalent events are also recognised in the Sorbas basin, which experienced a rapid deepening at the T/M boundary marked by the Azagador/Lower Abad transition and a second event with significant slumping at the Lower/Upper Abad limit (Krijgsman et al., 2001; Sierro et al., 2001).

Synchronous with the uplift of the Murcia–Cartagena basin, the Fortuna basin underwent major tectonic subsidence of about 20 cm/kyr (Fig. 9). The Tortonian II of the Lorca and Fortuna basins is also characterised by
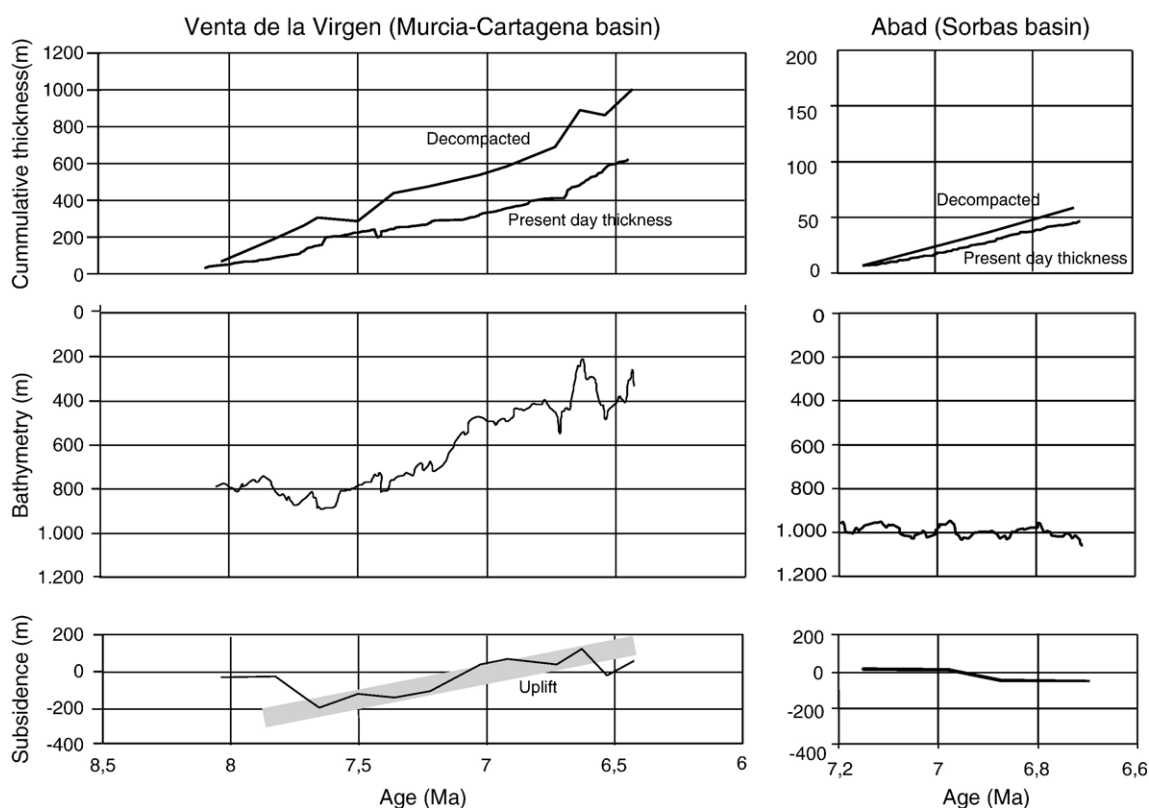

Fig. 8. Geohistory analysis of the Venta de la Virgen section and the Abad composite section. The decompaction curves are constructed from the present day thickness curve using initial thickness values and accounting for sediment accumulation. The bathymetry curves are constructed from a 5-point moving average of the actual P/B calculations. The subsidence curves are constructed by using backstripping techniques as described in the text. The gray area in the subsidence diagram of de Venta de la Virgen section indicates a continuous uplift rate of ∼30 cm/kyr between 7.8 and 6.6 Ma, while the depth of the Sorbas basin remains virtually unchanged during 7.2 till 6.7 Ma.
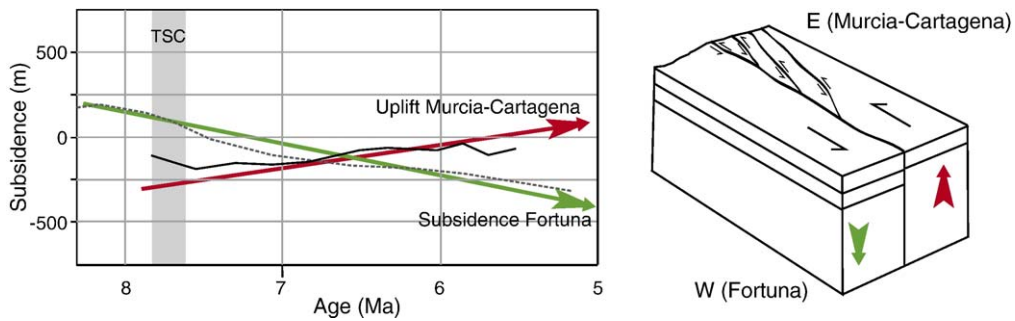
Fig. 9. Subsidence versus uplift of the Fortuna and Murcia–Cartagena basins during the interval of evaporite formation in the eastern Betics (TSC). It emphasises the differential vertical motion in the regions, which are most likely related to tectonic activity along the Alhama de Murcia fault zone. On the right-hand side is a schematical representation of the Alhama de Murcia Fault, when acting as a reverse strike-slip fault. This could explain the observed synchronous subsidence in Fortuna and uplift in Murcia–Cartagena, and the development of a threshold that could lead to evaporitic conditions in the Fortuna region.

open marine marls, and palaeomagnetic data show that they at least comprise the time interval between 8.3 and 7.8 Ma (Dinarés-Turell et al., 1999; Krijgsman et al., 2000). Although subsidence continued, this region shows a gradual transition via diatomites and evaporites to continental deposits between 7.8 and 7.6 Ma, marked by a drastic change in basin configuration. Continuously ongoing subsidence furthermore accommodated a thick series of more than 1 km of Mio–Pliocene continental deposits (Garcés et al., 1998, 2001). In summary, the Fortuna basin experienced continuous subsidence, simultaneously with the Murcia–Cartagena basin being uplifted (Fig. 9). It is thus likely that these movements are related to the same geodynamic mechanism.

The main tectonic feature of the area is the Alhama de Murcia fault system, which is located between the Murcia–Cartagena basin and the Fortuna basin (Fig. 1). This fault system acts as a reverse strike-slip wrenching fault, creating uplifted duplexes in the middle of the system (Fig. 9). It was active during the Neogene and Quaternary and its fault movements are earlier suggested to have controlled the development of the Fortuna and Lorca basins from the Late Miocene onwards (Martínez-Díaz, 2002). The Alhama de Murcia fault thus also may have caused differential movements of the basins on both sides of the fault system as the uplifted duplexes could well be acting as the emerging thresholds, which cut off the connection to the Murcia–Cartagena basin and thus to the open marine environment. The differential vertical movements on both sides of the system i.e. subsidence of the Fortuna basin and uplift of the Murcia–Cartagena basin can also be accommodated by this fault if it not only acted as a strike-slip but also as a reverse fault (Fig. 9). Consequently, the tectonic emergence of the Carrascoy massif at the basin margin threshold may have caused the

restriction in water circulation between Mediterranean and Fortuna basin leading to the Tortonian Salinity Crisis of the Eastern Betics. The present-day topography of the Sierra de Carrascoy is mostly the result of a Pliocene to recent uplift (Sanz de Galdeano et al., 1998), indicating that uplift of the study area did not stop at 6.6 Ma, but has continued until today.

8. Conclusions

The integration of multi-disciplinary stratigraphic techniques allowed the construction of an accurate chronology for the marine sedimentary sequences of the Venta de la Virgen section in the Murcia–Cartagena basin. Planktonic foraminifera data reveal at least five major events that can be correlated to the Messinian astrochronologies of the Mediterranean sequences. The magnetostratigraphic polarity pattern is not very well established because of weak NRM intensities. Nevertheless, several palaeomagnetic reversals could be accurately pinpointed providing crucial age constraints, especially on the base and top of the section. $^{40}Ar/^{39}Ar$ dating results of 7.30 ± 0.08 and 7.66 ± 0.08 Ma on two volcanic levels provide extra age control. The results of the three independent dating methods are in good agreement with each other and show that the sediments of the Venta de la Virgen section have been deposited between 8.1 and 6.4 Ma, and that the sediment accumulation rate was rather constant (35 cm/kyr) from 8.1 till 6.7 Ma.

Palaeobathymetric data indicate that the depth of the Murcia–Cartagena gradually decreased from 8 to 6.7 Ma, while the depth of the Sorbas basin remained unchanged between 7.2 and 6.8 Ma. This implies that local tectonic activity dominates the differential vertical motions in the eastern Betics and that eustatic sea-level

changes are only of minor importance. Synchronous with tectonic uplift of the Murcia–Cartagena basin, the Fortuna basin underwent significant subsidence. This could be explained by reverse strike-slip wrench faulting along the Alhama de Murcia fault, which may thus have formed the threshold that caused restriction in water circulation between Mediterranean and Fortuna basin leading to the Tortonian Salinity Crisis of the Eastern Betics.

Acknowledgements

References

Andrieux, J., Fontboté, J.M., Mattauer, M., 1971. Sur un modèle explicatif de l'Arc de Gibraltar. Earth Planet. Sci. Lett. 12, 115–118.

Babel, M., 1999. History of sedimentation of the Nida Gypsum deposits (Middle Miocene Carpathian foredeep, southern Poland). Geol. 429–447.

Baggley, K.A., 2000. The Late Tortonian–Early Messinian foraminiferal record of the Abad Member (Turre Formation), Sorbas Basin, Almeria, South-East Spain. Palaeontology 43, 1069–1112.

Clauzon, G., Suc, J.P., Gautier, F., Berger, A., Loutre, M.F., 1996. Alternate interpretation of the Messinian salinity crisis: Controversy resolved? Geology 24, 363–366.

De Larouzière, F.D., Bolze, J., Bordet, P., Hernandez, J., Montenat, C., Ott d'Estevou, P., 1988. The Betic segment of the lithosperic Trans-Alboran shear zone during the Late Miocene. Tectonophysics 152, 41–52.

Dinarès-Turell, J., Sprovieri, R., Caruso, A., Stefano, E.D., Gomis-Coll, E., Pueyo, J.J., Rouchy, J.M., Taberner, C., 1999. Preliminary integrated magnetostratigraphic and biostratigraphic correlation in the Miocene Lorca basin, (Murcia SE Spain). Acta Geol. Hisp. 32, 161–171.

Dronkert, H., 1976. Late Miocene evaporites in the Sorbas Basin and adjoining areas. Mem. Soc. Geol. Ital. 16, 341–361.

Duggen, S., Hoernle, K., Van den Bogaard, P., Rüpke, L., Morgan, J.P., 2003. Deep roots of the Messinian salinity crisis. Nature 422, 602–606.

Evans, A.L., 1988. Neogene tectonics and stratigraphic events in the Gulf of Suez rift area, Egypt. Tectonophysics 153, 235–247.

Fortuin, A.R., Krijgsman, W., 2003. The Messinian of the Nijar Basin (SE Spain): sedimentation, depositional environments and paleogeographic evolution. Sediment. Geol. 160, 213–242.

Garcés, M., Krijgsman, W., Agustí, J., 1998. Chronology of the late Turolian deposits of the Fortuna basin (SE Spain): implications for the Messinian evolution of the eastern Betics. Earth Planet. Sci. Lett. 163, 69–81.

Garcés, M., Krijgsman, W., Agustí, J., 2001. Chronostratigraphic framework and evolution of the Fortuna basin (Eastern Betics) since the late Miocene. Basin Res. 13, 199–216.

Hilgen, F.J., Krijgsman, W., 1999. Cyclostratigraphy and astrochronology of the Tripoli diatomite Formation (pre-evaporite Messinian Sicily, Italy). Terra Nova 11, 16–22.

Hilgen, F.J., Krijgsman, W., Langereis, C.G., Lourens, L.J., Santarelli, A., Zachariasse, W.J., 1995. Extending the astronomical (polarity) time scale into the Miocene. Earth Planet. Sci. Lett. 136, 495–510.

Hilgen, F.J., Bissoli, L., Iaccarino, S., Krijgsman, W., Meijer, R., Negri, A., Villa, G., 2000. Integrated stratigraphy and astrochronology of the Messinian GSSP at Oued Akrech (Atlantic Morocco). Earth Planet. Sci. Lett. 182, 237–251.

Hodell, D.A., Curtis, J.H., Sierro, F.J., Raymo, M.E., 2001. Correlation of late Miocene to early Pliocene sequences between the Mediterranean and North Atlantic. Paleoceanography 16, 164–178.

Hsü, K.J., Ryan, W.B.F., Cita, M.B., 1973. Late Miocene desiccation of the Mediterranean. Nature 242, 240–244.

Kastens, K., 1992. Did a glacio-eustatic sealevel drop trigger the Messinian salinity crisis? New evidence from ODP SIte 654 in the Tyrrhenian Sea. Paleoceonography 7, 333–356.

Kirschvink, J.L., 1980. The least-squares line and plane and the analysis of palaeomagnetic data. Geophys. J. R. Astron. Soc. 62, 699–718.

Krijgsman, W., Garcés, M., 2004. Palaeomagnetic constraints on the geodynamic evolution of the Gibraltar Arc. Terra Nova 16, 281–287.

Krijgsman, W., Hilgen, F.J., Langereis, C.G., Santarelli, A., Zachariasse, W.J., 1995. Late Miocene magnetostratigraphy, biostratigraphy and cyclostratigraphy in the Mediterranean. Earth Planet. Sci. Lett. 136, 475–494.

Krijgsman, W., Hilgen, F.J., Raffi, I., Sierro, F.J., Wilson, D.S., 1999. Chronology, causes and progression of the Messinian salinity crisis. Nature 400, 652–655.

Krijgsman, W., Garcés, M., Agustí, J., Raffi, I., Taberner, C., Zachariasse, W.J., 2000. The "Tortonian salinity crisis" of the eastern Betics (Spain). Earth Planet. Sci. Lett. 181, 497–511.

Krijgsman, W., Fortuin, A.R., Hilgen, F.J., Sierro, F.J., 2001. Astrochronology for the Messinian Sorbas basin (SE Spain) and orbital (precessional) forcing for evaporite cyclicity. Sediment. Geol. 140, 43–60.

Krijgsman, W., Gaboardi, S., Hilgen, F.J., Iaccarino, S., Kaenel, E., Van der Laan, E., 2004. Revised astrochronology for the Ain el Beida section (Atlantic Morocco): No glacio-eustatic control for the onset of the Messinian Salinity Crisis. Newsl. Stratigr. 1, 87–101.

Kuiper, K.F., Krijgsman, W., Garcés, M., Wijbrans, J.R., in press. Revised isotopic (^{40}Ar/^{39}Ar) age for the lamproite volcano of Cabezos Negros, Fortuna Basin (Eastern Betics, SE Spain). Palaeogeogr. Palaeoclimatol. Palaeoecol.

López-Garrido, A.C., Rodriquez-Fernández, J., Sanz de Galdeano, C., 1998. Timing of major events in the Neogene geologic evolution of the Betic Cordillera (South Spain). Rom. J. Stratigr. 78, 107–114.

Martín, J.M., Braga, J.C., 1994. Messinian events in the Sorbas Basin in southeastern Spain and their implications in the recent history of the Mediterranean. Sediment. Geol. 90, 257–268.

Martínez-Díaz, J.J., 2002. Stress field variation related to fault interaction in a reverse oblique-slip fault: the Alhama de Murcia fault, Betic Cordillera, Spain. Tectonophysics 356, 291–304.

Montenat, C., 1973. Les formations Néogènes et Quaternaires du Levant espagnol (Provinces d'Alicante et de Murcia), PhD. Thesis, Orsay Univ., 1170 pp.

Montenat, C., 1990. Les bassins néogènes du domaine bétique oriental (Espagne): Tectonique et sédimentation dans un couloir de décrochement, Première partie: Etude régionale. Doc. et Trav. IGAL 12–13, 1–392.

Montenat, C., Ott d´Estevou, P., Coppier, G., 1990a. Les bassins néogènes entre Alicante et Cartagena. Doc. et Trav. IGAL 12–13, 313–368.

Montenat, C., Ott d'Estevou, P., Rodríguez-Fernández, J., Sanz de Galdeano, C., 1990b. Geodynamic evolution of the Betic Neogene intramontane basins (S and SE Spain). Paleontol. Evol. 2, 5–59.

Müller, D.W., Hsü, K.J., 1987. Event stratigraphy and paleoceanography in the Fortuna basin (Southeast Spain): a scenario for the Messinian salinity crisis. Paleoceanography 2, 679–696.

Perrier, R., Quibler, J., 1974. Thickness in sedimentary layers during compaction history; methods for quantitative evaluation. Am. Assoc. Pet. Geol. Bull. 58, 507–520.

Peryt, T.M., Peryt, D., Jasionowski, M., Poberezhskyy, A.V., Durakiewicz, T., 2004. Post-evaporitic restricted deposition in the Middle Miocene Chokrakian–Karaganian of East Crimea (Ukraine). Sediment. Geol. 170, 21–36.

Playà, E., 1998. Les evaporites de les conques bétiques marginals (Fortuna–Lorca, Miocè superior): Comparació amb altres conques mediterrànies. PhD. Thesis, Univ. Barcelona. 248 pp.

Playà, E., Ortí, F., Rosell, L., 2000. Marine to non-marine sedimentation in the upper Miocene evaporites of the Eastern Betics, SE Spain: sedimentological and geochemical evidence. Sediment. Geol. 133, 135–166.

Poisson, A.M., Morel, J.L., Andrieux, J., Coulon, M., Wernli, R., Guernet, C., 1999. The origin and development of Neogene basins in the SE Betic Cordillera (SE Spain): a case study of the Tabernas–Sorbas and Huercal Overa basins. J. Pet. Geol. 22, 97–114.

Renne, P.R., Swisher, C.C., Deino, A.L., Karner, D.B., Owens, T.L., DePaolo, D.J., 1998. Intercalibration of standards, absolute ages and uncertainties in ^{40}Ar/^{39}Ar dating. Chem. Geol. 145, 117–152.

Rosell, L., Orti, F., Kasprzyk, A., Playa, E., Peryt, T.M., 1998. Strontium geochemistry of Miocene primary gypsum: Messinian of southeastern Spain and Sicily and Badenian of Poland. J. Sediment. Res. 68, 63–79.

Rouchy, J.-M., Saint Martin, J.P., 1992. Late Miocene events in the Mediterranean as recorded by carbonate–evaporite relations. Geology 20, 629–632.

Rouchy, J.-M., Noël, D., Wali, A.M.A., Aref, M.A.M., 1995. Evaporitic and biosiliceous cyclic sedimentation in the Miocene of the Gulf of Suez — depositional and diagenetic aspects. Sediment. Geol. 94, 277–297.

Rouchy, J.M., Taberner, C., Blanc-Valleron, M.-M., Sprovieri, R., Russell, M., Pierre, C., Stefano, E.D., Pueyo, J.J., Caruso, A., Dinares-Turell, J., Gomis-Coll, E., Wolff, G.A., Cespuglio, G., Ditchfield, P., Pestrea, S., Combourieu-Nebout, N., Santisteban, C., Grimalt, J.O., 1998. Sedimentary and diagenetic markers of the restriction in a marine basin: the Lorca Basin (SE Spain) during the Messinian. Sediment. Geol. 121, 23–55.

Ryan, W.B.F., Hsü, K.J., et al., 1973. Initial Reports of the DSDP, vol. 13. U.S. Government Printing office, Washington DC. 514 pp.

Sanz de Galdeano, C., Vera, J.A., 1992. Stratigraphic record and palaeogeographical context of the Neogene basins in the Betic Cordillera, Spain. Basin Res. 4, 21–36.

Sanz de Galdeano, C., López-Garrido, A.C., García-Tortosa, F.J., 1998. Nuevos datos para la estimación de los valores de levantamiento desde el Tortoniense Superior a la actualidad en la parte centro-occidental de la Sierra de Carrascoy (provincia de Murcia). Geogaceta 23, 139–142.

Sierro, F.J., Hilgen, F.J., Krijgsman, W., Flores, J.A., 2001. The Abad composite (SE Spain): a Messinian reference section for the Mediterranean and the APTS. Palaeogeogr. Palaeoclimatol. Palaeoecol. 168, 141–169.

Stapel, G., Moeys, R., Biermann, C., 1996. Neogene evolution of the Sorbas basin (SE Spain) determined by paleostress analysis. Tectonophysics 255, 291–305.

Steckler, M.S., Watts, A.B., 1978. Subsidence of the Atlantic-type continental margin off. New York. Earth Planet. Sci. Lett. 41, 1–13.

Steiger, R.H., Jäger, E., 1977. Subcommission on geochemistry: convention on the use of decay constants in geo- and cosmochronology. Earth Planet. Sci. Lett. 36, 359–362.

Troelstra, S.R., Poel, H.M.v.d., Huisman, C.H.A., Geerlings, L.P.A., Dronkert, H., 1980. Paleoecological changes in the latest Miocene of the Sorbas Basin, SE Spain. Géol. Méditerr. 7, 115–126.

Van der Zwaan, G.J., Jorissen, F.J., De Stigter, H.C., 1990. The depth dependency of planktonic/benthonic foraminiferal ratios: constraints and applications. Mar. Geol. 95, 1–16.

Van Hinsbergen, D.J.J., Kouwenhoven, T.J., Van der Zwaan, G.J., 2005. Paleobathymetry in the backstripping procedure: correction for oxygenation effects on depth estimates. Palaeogeogr. Palaeoclimatol. Palaeoecol. 221, 245–265.

Van Hinte, J.E., 1978. Geohistory analysis — application of micropaleontology in exploration geology. Am. Assoc. Pet. Geol. Bull. 62, 201–222.

Vázquez, A., Utrilla, R., Zamarreno, Y., Sierro, F.J., Flores, J.A., Frances, G., Barcena, M.A., 1999. Precession related sapropelites of the Messinian Sorbas basin (South Spain): Paleoenvironmental significance. Palaeogeogr. Palaeoclimatol. Palaeoecol. 158, 353–370.

Weijermars, R., 1988. Neogene tectonics in the western Mediterranean may have caused the Messinian salinity crisis and an associated glacial event. Tectonophysics 148, 211–219.

Zijderveld, J.D.A., 1967. A.C. Demagnetization of rocks: analysis of results. In: Collinson, D.W., Creer, K.M., Runcorn, S.K. (Eds.), Methods in Palaeomagnetism. Elsevier, New York, pp. 254–286.